Ternary Metal Oxide Embedded Carbon Derived from Metal Organic Frameworks for Adsorption of Methylene Blue and Acid Red 73

Menglin Yu, Heng Dong, Yingdie Zheng, Weiping Liu

PII: S0045-6535(21)01038-9

DOI: https://doi.org/10.1016/j.chemosphere.2021.130567

Reference: CHEM 130567

To appear in: *ECSN*

Received Date: 4 December 2020

Revised Date: 5 April 2021

Accepted Date: 10 April 2021

Please cite this article as: Yu, M., Dong, H., Zheng, Y., Liu, W., Ternary Metal Oxide Embedded Carbon Derived from Metal Organic Frameworks for Adsorption of Methylene Blue and Acid Red 73, *Chemosphere*, https://doi.org/10.1016/j.chemosphere.2021.130567.

Ternary Metal Oxide Embedded Carbon Derived from Metal Organic Frameworks for Adsorption of Methylene Blue and Acid Red 73

Menglin Yu,[a,b,#] Heng Dong,[b,#] Yingdie Zheng,[a] and Weiping Liu[a,*]

Author contribution statement

Menglin Yu: Conceptualization, Methodology, Investigation, Data curation, Formal analysis, Writing - review & editing. **Heng Dong**: Investigation, Formal analysis, Writing - Original drafting and validation. **Yingdie Zheng**: Investigation. **Weiping Liu**: Funding acquisition, Resources, Project administration, Supervision.

[#]M. Yu and H. Dong contributed equally to the work.

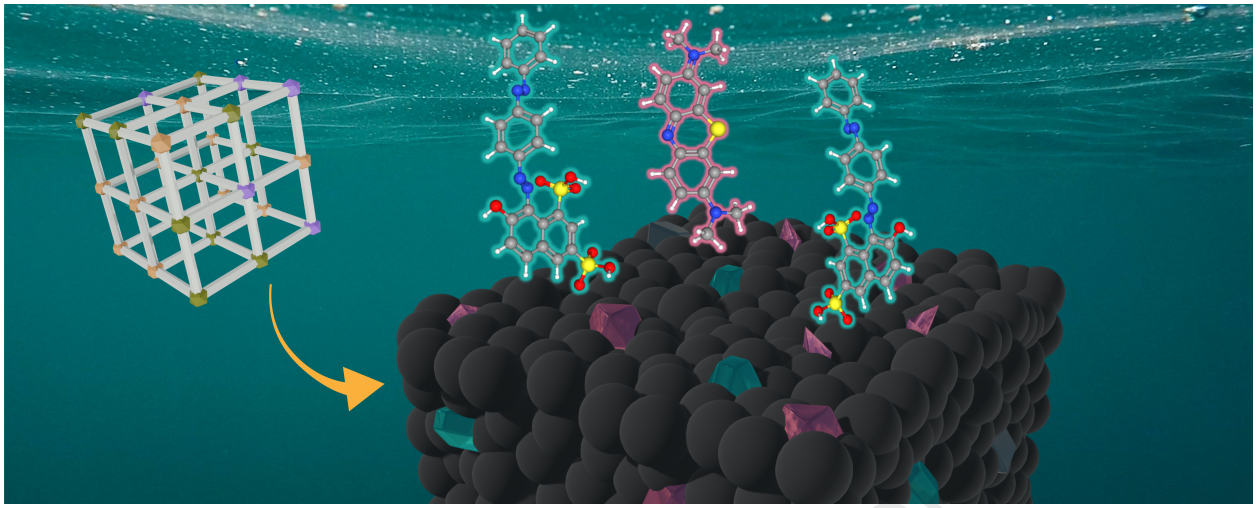

Ternary Metal Oxide Embedded Carbon Derived from Metal Organic Frameworks for Adsorption of Methylene Blue and Acid Red 73

Menglin Yu,[a,b,#] Heng Dong,[b,#] Yingdie Zheng,[a] and Weiping Liu[a,*]

[a]College of Environmental and Resource Science, Zhejiang University, Hangzhou 310058, China

[b]Linde + Robinson Laboratories, California Institute of Technology, Pasadena, California 91125, United States

***Corresponding Author: Weiping Liu**

College of Environmental and Resource Sciences, Zhejiang University

Hangzhou 310058, China

Tel: +86571-88982740

E-mail: wliu@zju.edu.cn

Highlights:

- Metal oxide embedded CMOFs-NH_2 were prepared by pyrolysis of MOF-NH_2 precursors.
- CMOF(Fe/Al/Ni 8/7/5)-NH_2 had ~20 times higher dye adsorption than AC in 10 min.
- CMOF(Fe/Al/Ni 8/7/5)-NH_2 efficiently adsorbed both cationic MB and anionic AR-73.
- Adsorption behavior of CMOFs-NH_2 was well accounted for by surface chemistry.
- A surface model was proposed for the performance of CMOF(Fe/Al/Ni 8/7/5)-NH_2.

Abstract

Organic dyes can enter water bodies through industrial wastes and may pose threat to the health of aquatic organisms and human. Metal organic framework derived carbon materials (CMOFs) have shown excellent performance for aqueous dye adsorption. However, few have studied multimetallic CMOFs for dye removal. Herein, a ternary metal oxide embedded carbon derived from amino-modified metal organic framework (CMOF(Fe/Al/Ni 8/7/5)-NH_2) has been developed as an efficient adsorbent to remove aqueous methylene blue (MB) and acid red 73 (AR-73). CMOF(Fe/Al/Ni 8/7/5)-NH_2 reached adsorption equilibrium for both MB and AR-73 within 30 min at neutral pH condition. It also achieved 18 and 24 times higher adsorption than commercial activated carbon (AC) in 10 min for MB and AR-73, respectively. Compared to other CMOFs-NH_2, CMOF(Fe/Al/Ni 8/7/5)-NH_2 had the highest adsorption capacity for both cationic MB and anionic AR-73. In addition, CMOF(Fe/Al/Ni 8/7/5)-NH_2 had < 0.15% metal leaching in 90 min in the pH range of 4-10, and it also maintained 89% and 95% adsorption capacity for MB and AR-73 in five consecutive adsorption batches, respectively. Electrostatic interaction was identified as the primary interaction between CMOFs-NH_2 and the dyes, and the embedded crystalline metal oxides with different points of zero charge (PZCs) were identified to be the key adsorption sites. A uniformly distributed surface charge model was proposed to explain the exceptional adsorption capacity of CMOF(Fe/Al/Ni 8/7/5)-NH_2. With fast kinetics, high adsorption capacity, wide applicability and good stability, CMOF(Fe/Al/Ni 8/7/5)-NH_2 may be an effective adsorbent for many other ionic organic pollutants.

Keywords: Cationic dye; Anionic dye; Fast adsorption; Carbon-based adsorbents; Metal organic

48 frameworks; Ternary metal oxides.

49

1. Introduction

Organic dyes, as introduced by painting, textile, electroplating, leather or paper industrial wastewater, are emerging as important aqueous pollutants, posing threat to the health of aquatic organisms and human being due to their solubility, toxicity, possible carcinogenic effects as well as interference of photosynthesis through absorption to incident light (Adeyemo et al., 2012; Katheresan et al., 2018; Kaur et al., 2019; Lellis et al., 2019). For example, methylene blue (MB), a common cationic dye, was found to cause eye irritation, vomiting, mental disorder, and has even been identified as a mutagen and carcinogen (Yao et al., 2010; Zhao et al., 2015; Xu et al., 2016). Common treatment techniques for dye wastewater include biological treatment, adsorption, coagulation, advanced oxidation, membrane filtration and photocatalysis (Gupta, 2009; Yagub et al., 2014; Ahmad et al., 2015). Among these, adsorption has been widely applied because of its high efficiency, low cost, easy and stable operation (Vandevivere et al., 1998; Allen et al., 2004; Yılmaz et al., 2016). In this regard, development of efficient, robust and cost-effective adsorbents is crucial.

So far, a number of adsorbents have been investigated for dye removal, including activated carbon, magnetic metal oxide nanoparticles, zeolite, graphene and graphene oxide (GO), carbon nanotubes (CNTs) (Meshko et al., 2001; Li et al., 2013; Ahmadijokani et al., 2020). Carbon-based materials have gained considerable attention because of their earth abundance, low toxicity as well as outstanding thermal and chemical properties (Pelekani and Snoeyink, 2000; Hameed et al., 2007; Ahmad et al., 2013; Gong et al., 2015). Metal organic frameworks (MOFs), as characterized by rich composition and structure, tunable porosity and large specific surface

area, serve as excellent templates for carbon-based adsorbents (Banerjee et al., 2012). MOF-derived carbon materials were shown to retain the metal centers, pore structure and large specific surface area of the MOF precursors and have found application in removal of aqueous pollutants (Yang et al., 2012; Li et al., 2014; Wang et al., 2020; Yu et al., 2020). Nanoporous carbon derived from ZIF-8 and Co-doped nanoporous carbon derived from ZIF-67 have shown good adsorptive performance for methylene blue (Torad et al., 2014; Abbasi et al., 2016). However, most reported adsorption processes on MOF-derived carbon adsorbents (denoted as CMOFs) could take up to several hours (Torad et al., 2014; Abbasi et al., 2016; Xu et al., 2017), leading to potential elevated cost for practical application. On the other hand, bimetallic and trimetallic adsorbents have been shown to have superior performance to their monometallic counterparts because of the synergistic effects of the metals (Wang et al., 2012; Mounfield III et al., 2016), but there have been few reports on multi-metal MOF-derived adsorbents.

Herein, a series of metal-oxide-embedded mesoporous carbon (CMOFs-NH_2) derived from amino-modified MOFs-NH_2 have been developed as efficient adsorbents for removal of cationic dye MB and anionic dye acid red 73 (AR-73). Specifically, various CMOFs-NH_2 were prepared by carbonizing the precursor MOFs-NH_2. Their adsorption performance was examined by adsorption kinetics, isotherms and the influence of ionic strength, temperature and pH. The adsorption mechanism was explored by measuring the Zeta potentials and points of zero charge (PZCs). The stability and reusability were demonstrated by ion leaching tests as well as adsorbent recovery and regeneration experiments. CMOF(Fe/Al/Ni 8/7/5)-NH_2 showed excellent adsorption rates for both cationic MB and anionic AR-73. The embedded metal oxides were

identified as important adsorption sites.

2. Materials and Methods

2.1. Materials

All chemicals were obtained from Sinopharm Chemical Reagent Co. Ltd. and were used without further purification. Solvents were HPLC grade unless otherwise stated. MB and AR-73 with chemical purity $\geqslant$ 97.0% (Sinopharm Chemical Reagent Co. Ltd.) were used in this study as model cationic and anionic dyes, respectively, with their structures and pKa given in **Table S1**. Activated carbon (AC, Sigma-Aldrich) was used as a benchmark.

2.2. Preparation of carbonized MOFs-NH_2 (CMOFs-NH_2)

For the synthesis of monometallic precursor MOFs-NH_2, including MIL-88(Fe)-NH_2, MIL-53(Al)-NH_2 and MOF(Ni)-NH_2, 4 mmol metal chloride or nitrate ($FeCl_3 \cdot 6H_2O$, $Al(NO_3)_3 \cdot 9H_2O$ and $Ni(NO_3)_2 \cdot 6H_2O$) and 4 mmol 2-aminoterephthalic acid were dissolved in 10 mL N, N-dimethylformamide (DMF) and transferred to a 30-mL microwave tube. The reaction was carried out at 150 °C for 40 min. After returning to room temperature without active cooling, the nanocrystals were separated by centrifugation at 11,000 rpm, washing with DMF and methanol and drying *in vacuo* at 150 °C for 12 h. Synthesis of multimetallic MOFs-NH_2 followed the same procedure except that mixed metal salts were used. Specifically, for bimetallic MOF(X/Y 1/1)-NH_2 (X, Y = Fe/Al/Ni), 2 mmol X and 2 mmol Y salts were used for synthesis. For MOF(Fe/Al/Ni 8/7/5)-NH_2 and MOF(Fe/Al/Ni 1/1/1)-NH_2, $FeCl_3 \cdot 6H_2O$, $Al(NO_3)_3 \cdot 9H_2O$ and $Ni(NO_3)_2 \cdot 6H_2O$ were used at molar ratios of 8:7:5 and 1:1:1, respectively, while total

amount of Fe, Al and Ni was kept 4 mmol.

The as-synthesized MOFs-NH_2 were pyrolyzed at 800 ºC for 2 h in N_2 to produce CMOFs-NH_2. Corresponding to the MOF-NH_2 precursors, CMOFs-NH_2 synthesized in the current study were designated as CMIL-88(Fe)-NH_2, CMIL-53(Al)-NH_2, CMOF(Ni)-NH_2, CMOF(Fe/Ni 1/1)-NH_2, CMOF(Al/Ni 1/1)-NH_2, CMOF(Fe/Al 1/1)-NH_2, CMOF(Fe/Al/Ni 8/7/5)-NH_2 and CMOF(Fe/Al/Ni 1/1/1)-NH_2, respectively.

2.3. Material characterization

The morphology of the MOFs-NH_2 and CMOFs-NH_2 was examined using a ZEISS Merlin field-emission scanning electron microscope (FE-SEM) and a FEI Tecnai G^2 F20 (200 kV) transmission electron microscope (TEM). The metal elemental composition was analyzed with an Oxford INCA X-MAX50 energy dispersive spectrometer (EDS) connected to the SEM. Powder X-ray diffraction (PXRD) patterns were collected using a Bruker D8 A25 X-ray diffractometer equipped with a Cu-Kα radiation (λ=1.5418 Å) source. The C and O content, as well as the chemical states of the materials were characterized by X-ray photoelectron spectroscopy (XPS) using Surface Science Instruments Thermo Scientific ESCALAB 250Xi surface spectrometer with monochromatic Al-Kα radiation (1486.6 eV). Brunauer-Emmett-Teller (BET) surface area and pore size distribution were determined through nitrogen adsorption and desorption isotherms taken by a gas adsorption instrument (Micromeritics 3Flex). Zeta potentials were recorded with a Zeta-potential analyzer (Nano ZS90, Malvern, UK).

2.4. Adsorption of dyes

All adsorption experiments were carried out at room temperature by adding 10 mg adsorbents

in 100 mL MB or AR-73 solution under continuous stirring at 150 rpm. For adsorption isotherms, 2 mL solution samples were collected after 12 h of contact time. The initial solution pH was adjusted by 1 M NaOH and 1 M H_2SO_4 before adding the adsorbents, while no buffer solution was used to maintain the pH during the adsorption process. The influence of ionic strength changes due to NaOH and H_2SO_4 addition was neglected. The adsorption isotherms were fitted to Langmuir (Equation 1) and Freundlich (Equation 2) models. c_e, q_e and q_m denote equilibrium adsorbate concentration in solution phase, adsorbent phase and the monolayer adsorption capacity, respectively. b is a constant related to free adsorption energy, while K_f and n are empirical constants. A trial-and-error procedure was used to determine the model parameters using the *Nonlinear Curve Fit* module in OriginPro 2018. MB and AR-73 concentrations were determined using a *JASCO* V-750 spectrophotometer at 508nm and 660nm, respectively. The quantity of AR-73 or MB absorbed onto CMOFs-NH_2 was calculated on the basis of the difference in solution concentration before and after adsorption.

$$c_e/q_e = 1/bq_m + c_e/q_m \quad (1)$$

$$q_e = K_f c_e^{1/n} \quad (2)$$

$$t/q_t = 1/v_0 + t/q_e \quad (3)$$

$$\ln(q_e - q_t) = lnq_e - k_1 t \quad (4)$$

For kinetic experiments, 1 mL solution samples were collected at certain time intervals. The kinetic data were fitted to pseudo second-order (Equation 3) and pseudo first-order (Equation 4) models. In both Equation 3 and 4, q_e and q_t denote the equilibrium adsorption amount and the amount adsorbed at time t, respectively. v_0 is the initial adsorption rate in Equation 3, and k_1 is

the pseudo first-order rate constant in Equation 4. The model parameters were also determined using *Nonlinear Curve Fit* module of OriginPro 2018.

2.5. Ion leaching tests and regeneration of adsorbents

Ion leaching experiments were performed at room temperature to test the stability of CMOF(Fe/Al/Ni 8/7/5)-NH_2. Specifically, 0.1 wt% CMOF(Fe/Al/Ni 8/7/5)-NH_2 suspensions were prepared and kept stirred at 150 rpm, with aliquots taken at certain time intervals. The suspension pH was adjusted with 1 M NaOH and 1 M H_2SO_4 solution. Leached ion concentration was determined by PerkinElmer NexION^{TM} 300X Inductively coupled plasma mass spectrometer (ICP-MS).

For adsorbent recovery and regeneration, 10 mg adsorbents were firstly suspended in 100 mL circum-neutral 100 mg L^{-1} AR-73 or MB solution for 12 h at room temperature to reach adsorption equilibrium. The spent adsorbents were subsequently recovered using a magnet and washed gently with milli-Q water (resistivity > 18.2 MΩ cm). Then, they were regenerated by sonication in 40 mL mixture of water/methanol (30/70, v/v) for 1h at room temperature. The regenerated adsorbents were collected by centrifugation and dried in a vacuum oven at 100 ˚C for 5 h for the next adsorption batch.

3. Results and Discussion

3.1. Material characteristics

The regular crystalline morphology of the as-synthesized MIL-88(Fe)-NH_2, MIL-53(Al)-NH_2 and MOF(Ni)-NH_2 was shown in **Figure S1**. Similar features were also noticed in

CMOF(Fe/Al/Ni 8/7/5)-NH_2 morphology (**Figure S2**). The synthesized MIL-53(Al)-NH_2 and MIL-88(Fe)-NH_2 possessed similar PXRD patterns to simulated MIL-53 and MIL-88 (Seoane et al., 2013; Yi et al., 2020), as shown in **Figure S3**. This indicated that -NH_2 groups had little effect on the integrity of the frameworks. After carbonization, the embedded Fe, Al and Ni in CMIL-88(Fe)-NH_2, CMIL-53(Al)-NH_2 and CMOF(Ni)-NH_2 were transformed into crystalline α-Fe_2O_3, NiO and γ-Al_2O_3, respectively **(Figure S4a)**. On the other hand, only NiO and Fe_3O_4 phases were identified from the XRD patterns of CMOF(Al/Ni 1/1)-NH_2 and CMOF(Fe/Al 1/1)-NH_2, respectively (**Figure S4b**), indicating the possible amorphous state of Al or doping of Al atoms in NiO and Fe_3O_4 lattice, consistent with previous study (Aghazadeh et al., 2017; Chen et al., 2018; Siddique et al., 2018; Ehsani et al., 2019). CMOF(Fe/Ni 1/1)-NH_2 consisted of both Fe_3O_4 and NiO phases, but it's worth noting that introduction of Al or Ni led to the formation of Fe_3O_4 in bimetallic CMOF(Fe/Al 1/1)-NH_2 and CMOF(Fe/Ni 1/1)-NH_2, in contrast to α-Fe_2O_3 in CMIL-88(Fe)-NH_2. Similar "missing" phase of Al was also observed in CMOF(Fe/Al/Ni 1/1/1)-NH_2 (**Figure S4c**). However, the PXRD pattern of CMOF(Fe/Al/Ni 8/7/5)-NH_2 consisted of a mixture of α-Fe_2O_3, Fe_3O_4, NiO and γ-Al_2O_3, indicating the influence of metal element composition on the final structure of CMOFs-NH_2. Monometallic and trimetallic CMOFs-NH_2 were used for further experiments.

The formation of crystalline metal oxides was confirmed by TEM images (**Figure S5**). The nanocrystals of NiO, γ-Al_2O_3, α-Fe_2O_3 and Fe_3O_4 in CMOF(Fe/Al/Ni 8/7/5)-NH_2 were well mixed at a sub-50-nm scale. The chemical states of the samples, as characterized by XPS spectra (**Figure S6**), also showed the formation of the metal oxides mentioned above.

Bimetallic metal oxides, including $NiFe_2O_4$, $FeAl_2O_4$, $NiAl_2O_4$ and $FeAlO_3$ could also be possible forms of the metal elements. However, synthesis of $NiFe_2O_4$ usually requires hydrothermal method (Satyanarayana et al., 2003; Zhou et al., 2005) or extended annealing time (Srivastava et al., 2009; Li et al., 2019), while the PXRD patterns of $FeAl_2O_4$ (Maiti et al., 2016), $NiAl_2O_4$ (Li et al., 2019) and $FeAlO_3$ (Santos et al., 2018) matched poorly with that of CMOF(Fe/Al/Ni 8/7/5)-NH_2 and CMOF(Fe/Al/Ni 1/1/1)-NH_2. Other bimetallic oxides such as $FeNi_2O_4$ and $AlFe_2O_4$ could also be excluded since they failed to match the valence states of the elements. Therefore, the embedded metal atoms in CMOF(Fe/Al/Ni 8/7/5)-NH_2 and CMOF(Fe/Al/Ni 1/1/1)-NH_2 primarily formed crystalline structures of individual metal oxides.

EDS mapping showed the uniform distribution of dopant Fe, Al and Ni in CMOF(Fe/Al/Ni 8/7/5)-NH_2 (**Figure S7**), consistent with the TEM images. The elemental composition of CMOFs-NH_2 was shown in **Table S2**. The metal element content ratios were generally consistent with their nominal ratios, while the total metal atomic percentage was kept ~12.5 at%. On the other hand, the O content varied from 24.5 at% for CMOF(Ni)-NH_2 to 30.9 at% for CMIL-53(Al)-NH_2. It is interesting to note that relatively lower O content was observed for Ni-containing CMOFs-NH_2 (e.g. 24.5 at% for CMOF(Ni)-NH_2, 26.8 at% for CMOF(Fe/Ni 1/1) -NH_2 and 24.7 at% for CMOF(Al/Ni 1/1)-NH_2) as opposed to their Fe- and Ni- containing counterparts (e.g. 30.7 at% for CMIL-53(Al)-NH_2, 30.4 at% for CMOF(Fe/Al 1/1)-NH_2 and 30.9 at% for CMIL-88(Fe)-NH_2). The difference was well accounted for by the stoichiometry of the embedded NiO, γ-Al_2O_3, α-Fe_2O_3 and Fe_3O_4, indicating that the oxidation state of the carbon lattice was relatively independent from the embedded metals.

The BET surface areas of CMOFs-NH_2 were shown in **Table S3**, and the pore structures of CMOFs-NH_2 and AC were also characterized by nitrogen adsorption-desorption isotherms (**Figure S8**). CMOFs-NH_2 had mainly mesoporous (pore size > 20 Å) structures. CMOF(Fe/Al/Ni 8/7/5)-NH_2 had mesopores concentrated at 70 Å and 176 Å, respectively, indicating its hierarchically porous structure. The other CMOFs-NH_2 showed similar pore distribution features with peak pore size around 60-70 Å. Commercial AC also had mesoporosity concentrated at 36 Å.

3.2. Adsorption Kinetics

The adsorption kinetics of CMOFs-NH_2 were measured with 40 mg L^{-1} initial dye concentration, with data shown in **Figure S9**. Fast MB and AR-73 uptake was observed between 0 and 10 min. Then the adsorption curves leveled off gradually. Generally, adsorption equilibrium was reached for both MB and AR-73 on CMOFs-NH_2 with 30 min, substantially faster than previously reported ZIF-67 derived Co-doped nanoporous carbon (Co/NPC-900) (Torad et al., 2014) and ZIF-8/dicyandiamide-derived nitrogen-doped porous carbon (Carbon-ZD) (Xu et al., 2017). On the contrary, AC showed no sign of reaching equilibrium within 90 min. The adsorption kinetic data of CMOFs-NH_2 for both MB and AR-73 followed pseudo second-order model (Equation 3) with R^2 > 0.97 shown in **Table 1**. On the other hand, the adsorption kinetics of the precursor MOFs-NH_2 for MB were also measured, with the data shown in **Figure S10** and fitted to pseudo first-order and pseudo second-order kinetic models in **Table S4**. Notably, CMOF(Fe/Al/Ni 8/7/5)-NH_2 had an adsorption of 1.15 mmol g^{-1} in 60 min, while under the same conditions MOF(Fe/Al/Ni 8/7/5)-NH_2 only had 0.37 mmol g^{-1}, indicating that

carbonization is a feasible strategy to further enhance the adsorption rates of MOFs-NH_2.

When comparing the adsorption kinetics of different CMOFs-NH_2, it was interesting to notice that Ni-containing CMOFs-NH_2 showed preferentially high adsorption rates for MB, while Fe- and Al-containing CMOFs-NH_2 showed high adsorption rates for AR-73. Specifically, for MB adsorption, the initial adsorption rate v_0 followed the order CMOF(Fe/Al/Ni 8/7/5)-NH_2 (37.22 mmol g^{-1} h^{-1}) > CMOF(Ni)-NH_2 (22.83 mmol g^{-1} h^{-1}) > CMOF(Fe/Al/Ni 1/1/1)-NH_2 (16.75 mmol g^{-1} h^{-1}) > CMIL-88(Fe)-NH_2 (13.01 mmol g^{-1} h^{-1}) > CMIL-53(Al)-NH_2 (7.39 mmol g^{-1} h^{-1}) (**Table 1**). In contrast, for AR-73 adsorption, v_0 followed the order CMOF(Fe/Al/Ni 8/7/5)-NH_2 (13.96 mmol g^{-1} h^{-1}) > CMIL-88(Fe)-NH_2 (8.02 mmol g^{-1} h^{-1}) > CMIL-53(Al)-NH_2 (5.08 mmol g^{-1} h^{-1}) > CMOF(Ni)-NH_2 (4.46 mmol g^{-1} h^{-1}) > CMOF(Fe/Al/Ni 1/1/1)-NH_2 (2.95 mmol g^{-1} h^{-1}). Generally speaking, the differences in adsorption rates are attributed to the porosity of the adsorbents as well as the adsorbent-adsorbate interactions. In this study, similar BET surface areas and pore distribution were observed for the CMOFs-NH_2 except CMOF(Fe/Al/Ni 8/7/5)-NH_2. Nonetheless, they still have substantially different adsorption rates, indicating that the adsorbent-adsorbate interactions were the primary contributor to the adsorption rates. On the other hand, CMOF(Fe/Al/Ni 8/7/5) had the highest adsorption rates for both MB and AR-73, while CMOF(Fe/Al/Ni 1/1/1)-NH_2 had only moderate adsorption rates, implying that the metal element composition had a substantial effect on the performance of trimetallic CMOFs-NH_2.

Table 1. Pseudo second-order kinetic parameters for adsorption of MB and AR-73 on CMOFs-NH_2 (C_0 = 40 mg L^{-1}, pH=7).

Kinetic parameters		CMIL-88(Fe)-NH_2	CMIL-53(Al)-NH_2	CMOF(Ni)-NH_2	CMOF(Fe/Al/Ni 1/1/1)-NH_2	CMOF(Fe/Al/Ni 8/7/5)-NH_2
MB adsorption	q_e (mmol g^{-1})	0.35	0.25	0.83	0.51	1.21
	v_0 (mmol g^{-1} h^{-1})	13.01	7.38	22.83	16.75	37.22
	R^2	0.993	0.974	0.980	0.991	0.993
AR-73 adsorption	q_e (mmol g^{-1})	0.26	0.16	0.13	0.11	0.45
	v_0 (mmol g^{-1} h^{-1})	8.02	5.08	4.46	2.95	13.96
	R^2	0.988	0.989	0.996	0.976	0.998

On AC, the adsorption kinetics of MB and AR-73 followed pseudo first-order model (Euation 4), as shown by the $R^2 > 0.99$ in **Table S5**. In terms of actual dye removal and water treatment, despite the large adsorption capacities of conventional carbonaceous adsorbents, it usually took hours or even days for the adsorption equilibrium to be established because of the slow adsorption kinetics (Hameed et al., 2007; Islam et al., 2017). This leads to extended contact time to meet the water quality requirement and hence elevated cost. CMOF(Fe/Al/Ni 8/7/5)-NH_2 achieved fast adsorption of 1.06 mmol g^{-1} and 0.38 mmol g^{-1} for MB and AR-73 within 10 min, respectively, which were 18 and 24 times higher than that of commercial AC (0.058 mmol g^{-1} for MB and 0.016 mmol g^{-1} for AR-73 in 10 min). This demonstrates that CMOF(Fe/Al/Ni 8/7/5)-NH_2 is an efficient adsorbent for aqueous dye removal. Therefore, reduced retention time and capital cost could be expected by employing CMOF(Fe/Al/Ni 8/7/5)-NH_2 in water treatment.

3.3. Adsorption Isotherms

The adsorption isotherms of CMOFs-NH_2 for MB and AR-73 were shown in **Figure 1a** and

1b. The isotherms were better fitted by Langmuir model ($R^2 > 0.98$) than Freundlich model, with the parameters shown in **Table 2**. The derived equilibrium adsorption capacities agreed well with those derived from the pseudo second-order kinetic model. For MB, the adsorption capacities of the various CMOFs-NH_2 followed the order CMOF(Fe/Al/Ni 8/7/5)-NH_2 (1.49 mmol g^{-1}) > CMOF(Ni)-NH_2 (0.85 mmol g^{-1}) > CMOF(Fe/Al/Ni 1/1/1)-NH_2 (0.56 mmol g^{-1}) > CMIL-88(Fe)-NH_2 (0.45 mmol g^{-1}) > CMIL-53(Al)-NH_2 (0.27 mmol g^{-1}). On the contrary, for AR-73, the adsorption capacities followed the order CMOF(Fe/Al/Ni 8/7/5)-NH_2 (0.47 mmol g^{-1}) > CMIL-88(Fe)-NH_2 (0.27 mmol g^{-1}) > CMIL-53(Al)-NH_2 (0.17 mmol g^{-1}) > CMOF(Ni)-NH_2 (0.14 mmol g^{-1}) ≈ CMOF(Fe/Al/Ni 1/1/1)-NH_2 (0.13 mmol g^{-1}). It is noticeable that the two orders not only deviate vastly from each other, but also disagree with the order of BET specific surface areas. This again indicated that the number of adsorption active sites for CMOFs-NH_2 was determined by not only the specific surface area, but also the chemical nature of the adsorbent surface. Meanwhile, the orders of adsorption capacities were consistent with that of initial adsorption rate v_0. CMOF(Fe/Al/Ni 8/7/5)-NH_2 showed excellent adsorption capacity for both cationic MB and anionic AR-73, demonstrating CMOF(Fe/Al/Ni 8/7/5)-NH_2 again as a versatile adsorbent. The adsorption capacity of CMOF(Fe/Al/Ni 8/7/5)-NH_2 was also 5 times higher than previously reported β-cyclodextrin functionalized magnetic nanoparticles (Zhou et al., 2016).

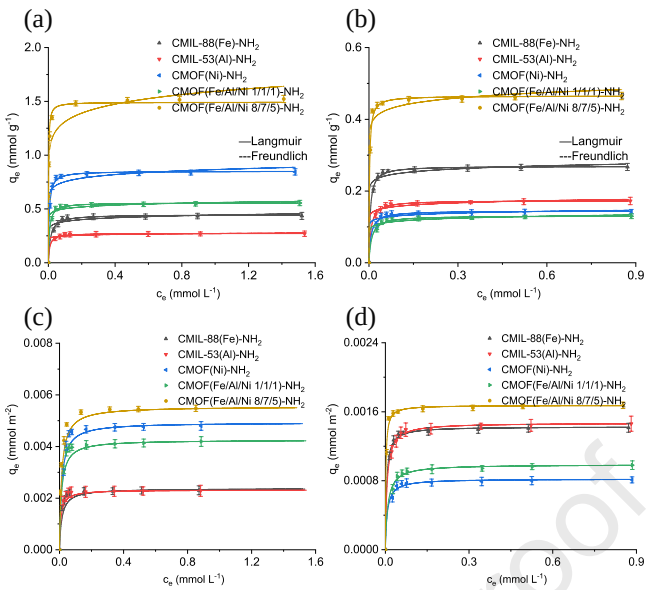

Figure 1. Adsorption isotherms of CMOFs-NH_2 normalized by the mass of adsorbents for (a) MB and (b) AR-73. The isotherms were fitted by Langmuir and Freundlich models. The adsorption isotherms were further normalized by the BET specific surface areas for (c) MB and (d) AR-73 to exclude the contribution of specific surface area to the adsorption capacities.

In order to exclude the contribution of specific surface areas and understand the effect of chemical nature of CMOFs-NH_2 surfaces on the adsorption capacity, the adsorption isotherms were normalized by BET surface areas in **Figure 1c and 1d**. The adsorption capacities of the various CMOFs-NH_2 for MB still followed the order CMOF(Fe/Al/Ni 8/7/5)-NH_2 (5.36 μmol m^{-2}) > CMOF(Ni)-NH_2 (4.83 μmol m^{-2}) > CMOF(Fe/Al/Ni 1/1/1)-NH_2 (4.23 μmol m^{-2}) > CMIL-88(Fe)-NH_2 (2.38 μmol m^{-2}) > CMIL-53(Al)-NH_2 (2.29 μmol m^{-2}). It's interesting to notice that Ni-containing CMOFs-NH_2 generally showed better adsorption capacity than their non-Ni-containing counterparts. On the other hand, the adsorption capacities for AR-73 following the order CMOF(Fe/Al/Ni 8/7/5)-NH_2 (1.69 μmol m^{-2}) > CMIL-53(Al)-NH_2 (1.44

304 μmol m^{-2}) ≈ CMIL-88(Fe)-NH_2 (1.43 μmol m^{-2}) > CMOF(Fe/Al/Ni 1/1/1)-NH_2 (0.98 μmol
305 m^{-2}) > CMOF(Ni)-NH_2 (0.80 μmol m^{-2}). Compared to the order obtained by normalizing the
306 adsorption capacity to mass, it's easy to discover the exchanged positions of CMIL-53(Al)-NH_2
307 with CMIL-88(Fe)-NH_2, as well as CMOF(Fe/Al/Ni 1/1/1)-NH_2 with CMOF(Ni)-NH_2. The
308 difference was because of the larger specific surface areas of CMIL-88(Fe)-NH_2 and
309 CMOF(Ni)-NH_2 compared with CMIL-53(Al)-NH_2 and CMOF(Fe/Al/Ni 1/1/1)-NH_2,
310 respectively.

311

312 **Table 2.** Langmuir and Freundlich model parameters for adsorption of MB and AR-73 on
313 CMOFs-NH_2 (pH=7).

Isotherm parameters		CMIL-88(Fe)-NH_2	CMIL-53(Al) -NH_2	CMOF (Ni)-NH_2	CMOF(Fe/Al/Ni 1/1/1)-NH_2	CMOF(Fe/Al/Ni 8/7/5)-NH_2
MB Langmuir constants	q_m (mmol g^{-1})	0.45	0.27	0.85	0.56	1.49
	b (L $mmol^{-1}$)	80.19	127.88	192.68	151.52	680.27
	R^2	0.991	0.998	0.997	0.996	0.994
MB Freundlich constants	K_f	0.44	0.27	0.87	0.56	1.59
	n^{-1}	15.94	26.87	16.56	21.30	11.84
	R^2	0.959	0.988	0.948	0.976	0.920
AR-73 Langmuir constants	q_m (mmol g^{-1})	0.27	0.17	0.14	0.13	0.47
	b (L $mmol^{-1}$)	234.19	161.81	147.28	115.07	531.91
	R^2	0.998	0.998	0.989	0.994	0.995
AR-73	K_f	0.28	0.18	0.15	0.13	0.49

Freundlich constants	n^{-1}	21.71	19.15	19.63	15.61	21.23
	R^2	0.982	0.985	0.972	0.976	0.958

For adsorption of both MB and AR-73, the adsorption capacities of the CMOFs-NH_2 still varied by a factor over 2 after normalized to the BET specific surface areas. Since the differences were attributed to adsorbent-adsorbate interactions, this indicated that different embedded metals in the CMOFs-NH_2 induced significantly different surface properties of the adsorbents. CMOF(Fe/Al/Ni 8/7/5)-NH_2 showed the highest adsorption capacity with the adsorption capacity normalized to BET specific surface area, while the adsorption capacity of CMOF(Fe/Al/Ni 1/1/1)-NH_2 was significantly inferior, indicating the importance of metal element composition for the adsorption performance of CMOFs-NH_2.

3.4. Effect of ionic strength and temperature on adsorption capacity of CMOF(Fe/Al/Ni 8/7/5)-NH_2

Since high salt concentration is often observed in industrial dye wastewater, the influence of salt concentration on the adsorption performance of CMOF(Fe/Al/Ni 8/7/5)-NH_2 was studied (**Figure S11**). Specifically, the equilibrium adsorption of MB and AR-73 by CMOF(Fe/Al/Ni 8/7/5)-NH_2 was measured in the presence of NaCl or Na_2SO_4 with a dye concentration of 40 or 200 mg L^{-1}. As shown in **Figure S11**, NaCl and Na_2SO_4 in the concentration range of 0-0.2 M had no significant impact on the adsorption capacity of CMOF(Fe/Al/Ni 8/7/5)-NH_2 for MB and AR-73. According to previous studies (Wang et al., 2010; Wu et al., 2014), this was because the dissolved salts screened the electrostatic interaction between CMOF(Fe/Al/Ni 8/7/5)-NH_2 and

the dyes but also promoted the charging of the dye molecules, which finally canceled out and had little net effect on the adsorption capacity. On the other hand, the equilibrium adsorption of MB increased when the initial MB concentration was increased from 40 mg L^{-1} to 200 mg L^{-1}. This was because of the enhanced mass transfer and stronger driving force of adsorption induced by the elevated MB concentration (Wu et al., 2014). However, increasing AR-73 initial concentration didn't increase the equilibrium adsorption amount, since the adsorbed amount with 40 mg L^{-1} initial AR-73 (0.47 mmol g^{-1}) has reached saturation (**Table 2**). In the meantime, temperature also showed a pronounced effect on the adsorption capacity (**Figure S12**). The adsorption isotherms at different temperatures for both MB and AR-73 were all well-fitted by Langmuir model, as shown by the $R^2 > 0.99$ (**Table S6**). When the temperature increased from 298 K to 318 K, the adsorption capacity of CMOF(Fe/Al/Ni 8/7/5)-NH_2 increased from 1.49 mmol g^{-1} to 1.74 mmol g^{-1}. This implied that the adsorption processes are endothermic.

3.5. Adsorption mechanism of CMOFs-NH_2

Unraveling the adsorbent-adsorbate interaction and adsorption active sites is essential for the understanding and design of CMOFs-NH_2. In order to understand the adsorption mechanism of CMOFs-NH_2 for MB and AR-73, the influence of pH on the adsorption capacity of CMOF(Fe/Al/Ni 8/7/5)-NH_2 was measured with a dye concentration of 100 mg L^{-1} (**Figure S13**). Increasing pH led to monotonic increase in the adsorption capacity for MB and decrease in that for AR-73, with sharp changes in the adsorption capacity observed in the pH range of 5-7. The adsorption capacity of CMOF(Fe/Al/Ni 8/7/5)-NH_2 for MB at pH 13 (1.78 mmol g^{-1}) was about 5 times of that at pH 1 (0.34 mmol g^{-1}). Similarly, the adsorption capacity for AR-73 at pH 1

(1.05 mmol g^{-1}) was also about 5 times of that at pH 13 (0.22 mmol g^{-1}). The drastic change in adsorption capacity with varying pH indicated that surface charging may play an important role for the adsorption.

This was well-accounted for by the electrostatic interaction of dye molecules with the surface of CMOF(Fe/Al/Ni 8/7/5)-NH_2. MB, with a pKa of ~3.1, takes on a singly charged cation form in solution with pH > 3.1, and gets protonated in acidic environment into doubly charged cationic form (Zhou et al., 2016). The two pKa values of AR-73 were predicted to be -3.03 and 0.19 (Swain, 2012) by Chemicalize developed by ChemAxon, respectively, indicating the anionic form of AR-73 in the surveyed pH range. On the other hand, the charging of CMOF(Fe/Al/Ni 8/7/5)-NH_2 surface was studied by Zeta potential measurement (**Figure 2a**). CMOF(Fe/Al/Ni 8/7/5)-NH_2 had a Zeta potential of 4.89 mV at pH 5 and -25.34 mV at pH 7. Therefore, the PZC of CMOF(Fe/Al/Ni 8/7/5)-NH_2 could be determined to be ~5.3 by using linear approximation between pH 5 and 7. This implied that the surface of CMOF(Fe/Al/Ni 8/7/5)-NH_2 was overall positively charged at pH below 5.3 and overall negatively charged at pH above 5.3. At acidic conditions, the positively charged surface had low affinity for positively charged MB because of electrostatic repulsion. Lower pH resulted in more positively charged CMOF(Fe/Al/Ni 8/7/5)-NH_2 surface and stronger repulsion, leading to smaller adsorption capacity for MB. As pH exceeded the PZC, the surface of CMOF(Fe/Al/Ni 8/7/5)-NH_2 became negatively charged, leading to a sharp rise in its affinity for MB. Further increase in pH induced more negatively charged adsorbent surface and higher adsorption capacity. The adsorption behavior of negatively charged AR-73 was accounted for in the same way. Therefore, it was

concluded that electrostatic interaction played the utmost role in the interaction of CMOF(Fe/Al/Ni 8/7/5)-NH_2 with MB and AR-73.

Surface acid-base chemistry also provided insight into the roles of embedded oxides of Fe, Al and Ni. As shown by XRD, XPS and TEM, the embedded Fe in CMOF(Fe/Al/Ni 8/7/5)-NH_2 was in the form of α-Fe_2O_3 and Fe_3O_4, while Al was in the form of γ-Al_2O_3 and Ni in the form of NiO. The PZCs of the embedded metal oxides were summarized in **Table S7**. NiO, with a PZC as low as 3.5-4 (Hernandez et al., 2005), was negatively charged under neutral pH condition, which enabled it to possess high affinity to positively charged MB. On the contrary, γ-Al_2O_3 had a PZC as high as 8.5-9.5 (Ruiz-Reina et al., 2003; Moreau et al., 2013), rendering itself as a positively charged adsorption site at neutral conditions with high affinity to negatively charged AR-73. In terms of the embedded Fe, the PZC of α-Fe_2O_3 may range from 8.3-9.5 (Penners et al., 1986; Gunnarsson et al., 2000; Gunnarsson et al., 2001), similar to that of γ-Al_2O_3, while Fe_3O_4 had a circum-neutral PZC of 6.8-6.9 (Regazzoni et al., 1983; Blesa et al., 1984). Hence, at neutral pH condition Fe_3O_4 sites didn't contribute significantly to the adsorbent-adsorbate interaction, while α-Fe_2O_3 was expected to possess high affinity to AR-73. Therefore, it was speculated that the embedded NiO was the adsorption center for MB while the γ-Al_2O_3 and α-Fe_2O_3 were the adsorption centers for AR-73.

This hypothesis was confirmed by measuring the change in Zeta potential of CMIL-88(Fe)-NH_2, CMIL-53(Al)-NH_2 and CMOF(Ni)-NH_2 after dye adsorption (**Figure 2b-d**). The initial of CMIL-88(Fe)-NH_2, CMIL-53(Al)-NH_2 and CMOF(Ni)-NH_2 were determined to be 9.8, 9.8 and 3.6, respectively, consistent with the PZCs of α-Fe_2O_3, γ-Al_2O_3 and NiO,

respectively. Adsorption of MB induced only a minor change of the PZCs of CMIL-88(Fe)-NH_2, CMIL-53(Al)-NH_2, indicating the weak electrostatic interactions. Since the adsorption of MB was contributed by both the embedded metal oxides and the carbon lattice, this implied that neither the embedded oxides of Fe and Al, nor the carbon lattice, had high affinity to MB. However, MB adsorption increased the PZC of CMOF(Ni)-NH_2 from 3.6 to 5.3, indicating the strong electrostatic interaction and the formation of inner-sphere complexes (Jordan et al., 2014). On the contrary, adsorption of AR-73 led to substantial decrease in the PZCs of both CMIL-88(Fe)-NH_2 (from 9.8 to 8.2) and CMIL-53(Al)-NH_2 (from 9.8 to 7.8), but no significant change in that of CMOF(Ni)-NH_2. This confirms that the embedded NiO in CMOFs-NH_2 functioned as adsorption centers for MB, while the α-Fe_2O_3, γ-Al_2O_3 functioned as adsorption centers for AR-73. The results also indicated that the carbon lattice didn't contribute significantly to the adsorption.

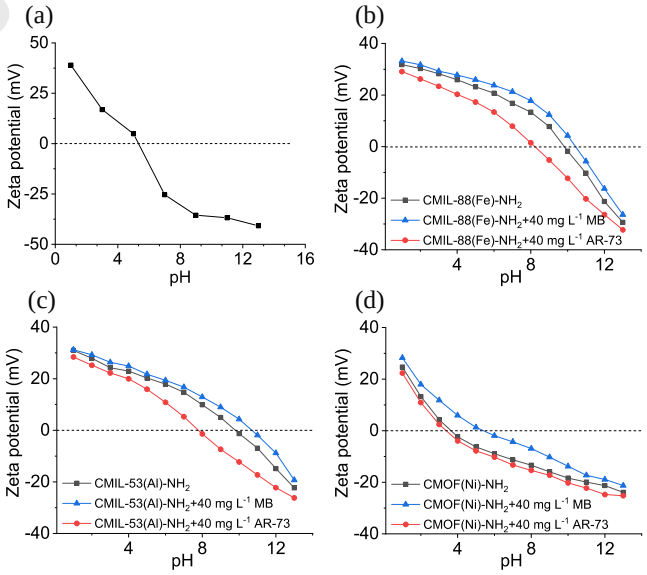

Figure 2. Zeta potential of (a) CMOF(Fe/Al/Ni 8/7/5)-NH_2, (b) CMIL-88(Fe)-NH_2, (c)

411 CMIL-53(Al)-NH_2 and (d) CMOF(Ni)-NH_2 as a function of pH.

412

413 In contrast to CMOF(Fe/Al/Ni 8/7/5)-NH_2 that showed excellent adsorption performance for
414 both MB and AR-73, CMOF(Fe/Al/Ni 1/1/1)-NH_2 failed to contain crystalline α-Fe_2O_3 and
415 γ-Al_2O_3, leading to compromised adsorption rates and capacity for AR-73. This implied that the
416 adsorption performance of CMOFs-NH_2 relied heavily on the formation of crystalline metal
417 oxides with appropriate PZCs to function as active adsorption sites for the dyes. In addition, this
418 also showed the significant tuning effect of metal element composition on the performance of
419 formed CMOFs-NH_2.

420 In spite of the crystalline metal oxides being identified as the active adsorption sites in
421 CMOFs-NH_2, this was unable to fully account for the outstanding adsorption performance of
422 CMOF(Fe/Al/Ni 8/7/5)-NH_2. For example, according to **Table S2**, the mass fractions of Ni in
423 CMOF(Ni)-NH_2 and CMOF(Fe/Al/Ni 8/7/5)-NH_2 were calculated to be 39% and 10%,
424 respectively. Since NiO was proposed as the adsorption site for MB, CMOF(Ni)-NH_2 should
425 have better adsorption performance for MB than CMOF(Fe/Al/Ni 8/7/5)-NH_2. In fact, this was
426 not consistent with the experimental results in that CMOF(Fe/Al/Ni 8/7/5)-NH_2 showed both
427 higher adsorption capacity and faster adsorption kinetics for MB compared to CMOF(Ni)-NH_2.
428 This might be due to the steric effect of MB, as shown in **Scheme S1**. Specifically, the positive
429 charge of MB tends to be smeared out to the whole molecule due to the conjugation effect. At
430 neutral pH, uniformly distributed negative charge of CMOF(Ni)-NH_2 would then lead to
431 "side-on" adsorption of MB molecules, which could block more adsorption sites and lower the

efficiency of adsorption in general. In contrast, based on EDS mapping (**Figure S3**) and TEM (**Figure S5**) results, CMOF(Fe/Al/Ni 8/7/5)-NH_2 had a heterogeneous surface with uniformly distributed hetero-charged sites, where negatively charged NiO sites were separated by positively charged γ-Al_2O_3 and α-Fe_2O_3 sites. The positively charged "dividers" on the surface favored the "end-on" adsorption because of their repulsion with positively charged MB molecules, thus facilitating the full usage of adsorption sites. As a result, despite the lower Ni content and less negatively charged sites in CMOF(Fe/Al/Ni 8/7/5)-NH_2 compared to CMOF(Ni)-NH_2, a higher adsorption capacity was observed for the former. The similar adsorption capacity of CMOF(Fe/Al/Ni 8/7/5)-NH_2 to CMIL-53(Al)-NH_2 for AR-73 could be accounted for in the same way. This also implied that uniform distribution of hetero-charged sites to be an efficient strategy to enhance the adsorption capacity of carbon-based adsorbents.

3.6. Regeneration of Adsorbents

Ion leaching tests and adsorbent regeneration tests were performed to study the stability and reusability of CMOF(Fe/Al/Ni 8/7/5)-NH_2. Specifically, ion leaching tests were performed in 0.1 wt% CMOF(Fe/Al/Ni 8/7/5)-NH_2 suspension at pH 4, 7 and 10 (**Figure S14**). The influence of MB and AR-73 adsorption on the ion leaching was studied with a dye concentration of 40 mg L^{-1}. Generally, the highest metal leaching was observed at pH 4 condition, and addition of MB **(Figure S14 d-f)** and AR-73 **(Figure S14 g-i)** to the suspension had no significant impact on the metal leaching. For all conditions, the leached metal concentration was well below 15 µg L^{-1} in 90 min. Therefore, the use CMOF(Fe/Al/Ni 8/7/5)-NH_2 causes little heavy metal contamination. On the other hand, the metal leaching was also quantified based on the leached metal percentage

(**Figure S14 j-l**). At pH 4, only 0.07% Fe, 0.14% Al and 0.14% Ni were leached over 90 min. These results demonstrated CMOF(Fe/Al/Ni 8/7/5)-NH_2 to be a highly stable adsorbent for MB and AR-73 over a wide pH range.

Furthermore, the used CMOF(Fe/Al/Ni 8/7/5)-NH_2 was successfully recovered using a magnet (**Figure S15a**). The adsorption capacity, which was measured in 100 mg L^{-1} dye solutions, remained 89% and 95% over five consecutive batches for both MB and AR-73, respectively (**Figure S15b**), confirming the reusability of CMOF(Fe/Al/Ni 8/7/5)-NH_2 in practical applications.

Considering the large adsorption capacity, fast adsorption kinetics, high stability and applicability for both cationic and anionic dyes, CMOF(Fe/Al/Ni 8/7/5)-NH_2 may serve as a promising candidate for adsorptive removal of aqueous dyes and water remediation.

4. Conclusion

In this study, we studied the adsorption performance of MOF-derived ternary metal oxide embedded carbon for aqueous MB and AR-73 adsorption. CMOFs-NH_2 achieved quick adsorption–for both MB and AR-73, with equilibrium established within 30 min at neutral pH condition. Notably, CMOF(Fe/Al/Ni 8/7/5)-NH_2 obtained 18 and 24 times higher adsorption than commercial–AC in 10 min for MB and AR-73, respectively. Meanwhile, CMOF(Fe/Al/Ni 8/7/5)-NH_2 had the largest adsorption capacity for both MB (1.49 mmol g^{-1}) and AR-73 (0.47 mmol g^{-1}) compared to the other CMOFs-NH_2. At the same time, CMOF(Fe/Al/Ni 8/7/5)-NH_2 was demonstrated stable by < 0.15% metal ion leaching in the pH range of 4-10 in 90 min, and it

maintained 89% and 95% adsorption capacity for MB and AR-73 in five consecutive adsorption batches, respectively.

On the other hand, electrostatic interaction was identified as the primary interaction of CMOFs-NH_2 with the dyes. Based on the different PZCs and Zeta potential measurement, the embedded NiO was recognized as the negatively charged adsorption site for MB, while α-Fe_2O_3 and γ-Al_2O_3 were recognized as positively charged adsorption sites for AR-73. A uniformly distributed surface charge model was proposed to understand the exceptional adsorption capacity of CMOF(Fe/Al/Ni 8/7/5)-NH_2. In addition to dyes, CMOF(Fe/Al/Ni 8/7/5)-NH_2 may also serve as an efficient adsorbent for other aqueous ionic pollutants.

Author contribution statement

Menglin Yu: Conceptualization, Methodology, Investigation, Data curation, Formal analysis, Writing - review & editing. **Heng Dong**: Investigation, Formal analysis, Writing - Original drafting and validation. **Yingdie Zheng**: Investigation. **Weiping Liu**: Funding acquisition, Resources, Project administration, Supervision.

[#]M. Yu and H. Dong contributed equally to the work.

Declaration of competing interest

The authors declare no competing financial interest.

Acknowledgment

This work was supported by National Natural Science Foundations of China (Grant No. 21777137). The authors would also like to thank China Scholarship Council for the support.

References

Abbasi, Z., Shamsaei, E., Leong, S.K., Ladewig, B., Zhang, X., Wang, H., 2016. Effect of carbonization temperature on adsorption property of ZIF-8 derived nanoporous carbon for water treatment. Microporous Mesoporous Mater. 236, 28-37.

Adeyemo, A.A., Adeoye, I.O., Bello, O.S., 2012. Metal organic frameworks as adsorbents for dye adsorption: overview, prospects and future challenges. Toxicol. Environ. Chem. 94, 1846-1863.

Aghazadeh, M., Karimzadeh, I., Ganjali, M.R., Malekinezhad, A., 2017. Al^{3+} doped Fe_3O_4 nanoparticles: a novel preparation method, structural, magnetic and electrochemical characterizations. Int. J. Electrochem. Sci. 12, 8033-8044.

Ahmad, A., Idris, A., Hameed, B., 2013. Organic dye adsorption on activated carbon derived from solid waste. Desalination Water Treat. 51, 2554-2563.

Ahmad, A., Mohd-Setapar, S.H., Chuong, C.S., Khatoon, A., Wani, W.A., Kumar, R., Rafatullah, M., 2015. Recent advances in new generation dye removal technologies: novel search for approaches to reprocess wastewater. RSC Adv. 5, 30801-30818.

Ahmadijokani, F., Mohammadkhani, R., Ahmadipouya, S., Shokrgozar, A., Rezakazem, M., Molavi, H., Aminabhavi, T.M., Arjmand, M., 2020. Superior chemical stability of UiO-66 metal-organic frameworks (MOFs) for selective dye adsorption. Chem. Eng. J., 125346.

Allen, S., Mckay, G., Porter, J.F., 2004. Adsorption isotherm models for basic dye adsorption by peat in single and binary component systems. J. Colloid Interface Sci. 280, 322-333.

Banerjee, A., Gokhale, R., Bhatnagar, S., Jog, J., Bhardwaj, M., Lefez, B., Hannoyer, B., Ogale, S., 2012. MOF derived porous carbon-Fe_3O_4 nanocomposite as a high performance, recyclable environmental superadsorbent. J. Mater. Chem. A 22, 19694-19699.

Blesa, M.A., Figliolia, N.M., Maroto, A.J., Regazzoni, A.E., 1984. The influence of temperature on the interface magnetite-aqueous electrolyte solution. J. Colloid Interface Sci. 101, 410-418.

Chen, J., Peng, X., Song, L., Zhang, L., Liu, X., Luo, J., 2018. Facile synthesis of Al-doped NiO nanosheet arrays for high-performance supercapacitors. Royal Soc. Open Sci. 5, 180842.

Ehsani, M., Esmaeili, S., Aghazadeh, M., Kameli, P., Tehrani, F.S., Karimzadeh, I., 2019. An investigation on the impact of Al doping on the structural and magnetic properties of Fe_3O_4 nanoparticles. Appl. Phys. A 125, 280.

Gong, J., Liu, J., Chen, X., Jiang, Z., Wen, X., Mijowska, E., Tang, T., 2015. Converting real-world mixed waste plastics into porous carbon nanosheets with excellent performance in the adsorption of an organic dye from wastewater. J. Mater. Chem. A 3, 341-351.

Gunnarsson, M., Jakobsson, A.-M., Ekberg, S., Albinsson, Y., Ahlberg, E., 2000. Sorption studies of cobalt (II) on colloidal hematite using potentiometry and radioactive tracer technique. J. Colloid Interface Sci. 231, 326-336.

Gunnarsson, M., Rasmusson, M., Wall, S., Ahlberg, E., Ennis, J., 2001. Electroacoustic and potentiometric studies of the hematite/water interface. J. Colloid Interface Sci. 240, 448-458.

Gupta, V., 2009. Application of low-cost adsorbents for dye removal-a review. J. Environ. Manage. 90, 2313-2342.

Hameed, B., Din, A.M., Ahmad, A., 2007. Adsorption of methylene blue onto bamboo-based activated carbon: kinetics and equilibrium studies. J. Hazard. Mater. 141, 819-825.

Hernandez, N., Moreno, R., Sanchez-Herencia, A.J., Fierro, J.L., 2005. Surface behavior of nickel powders in aqueous suspensions. J. Phys. Chem. B 109, 4470-4474.

Islam, M.A., Sabar, S., Benhouria, A., Khanday, W., Asif, M., Hameed, B., 2017. Nanoporous activated carbon prepared from karanj (Pongamia pinnata) fruit hulls for methylene blue adsorption. J. Taiwan Inst. Chem. Eng. 74, 96-104.

Jordan, N., Ritter, A., Scheinost, A.C., Weiss, S., Schild, D., Hübner, R., 2014. Selenium (IV) uptake by maghemite (γ-Fe_2O_3). Environ. Sci. Technol. 48, 1665-1674.

Katheresan, V., Kansedo, J., Lau, S.Y., 2018. Efficiency of various recent wastewater dye removal methods: a review. J. Environ. Chem. Eng. 6, 4676-4697.

Kaur, D., Bagga, V., Behera, N., Thakral, B., Asija, A., Kaur, J., Kaur, S., 2019. SnSe/SnO_2 nanocomposites: novel material for photocatalytic degradation of industrial waste dyes. Adv. Compos. Mater. 2, 763-776.

Lellis, B., Fávaro-Polonio, C.Z., Pamphile, J.A., Polonio, J.C., 2019. Effects of textile dyes on health and the environment and bioremediation potential of living organisms. Biotechnol. Res. Innovation 3, 275-290.

Li, D., Li, Y., Liu, X., Guo, Y., Pao, C., Chen, J., Hu, Y., Wang, Y., 2019. $NiAl_2O_4$ spinel supported Pt catalyst: high performance and origin in aqueous-phase reforming of methanol. ACS Catal. 9, 9671-9682.

Li, J., Li, S., Tang, Y., Li, K., Zhou, L., Kong, N., Lan, Y., Bao, J., Dai, Z., 2014. Heteroatoms ternary-doped porous carbons derived from MOFs as metal-free electrocatalysts for oxygen reduction reaction. Sci. Rep. 4, 1-8.

Li, Y., Du, Q., Liu, T., Peng, X., Wang, J., Sun, J., Wang, Y., Wu, S., Wang, Z., Xia, Y., 2013. Comparative study of methylene blue dye adsorption onto activated carbon, graphene oxide, and carbon nanotubes. Chem. Eng. Res. Des. 91, 361-368.

Maiti, S., Llorca, J., Dominguez, M., Colussi, S., Trovarelli, A., Priolkar, K.R., Aquilanti, G., Gayen, A., 2016. Combustion synthesized copper-ion substituted $FeAl_2O_4$ ($Cu_{0.1}Fe_{0.9}Al_2O_4$): A superior catalyst for methanol steam reforming compared to its impregnated analogue. J. Power Sources 304, 319-331.

Meshko, V., Markovska, L., Mincheva, M., Rodrigues, A., 2001. Adsorption of basic dyes on granular acivated carbon and natural zeolite. Water Res. 35, 3357-3366.

Moreau, P., Colette-Maatouk, S., Gareil, P., Reiller, P.E., 2013. Modelling of the adsorption of phenolic acids onto α, γ-alumina particles. Colloids Surf. A Physicochem. Eng. Asp. 435, 97-108.

Mounfield III, W.P., Taborga Claure, M., Agrawal, P.K., Jones, C.W., Walton, K.S., 2016. Synergistic effect of mixed oxide on the adsorption of ammonia with metal-organic frameworks. J. Ind. Eng. Chem. 55, 6492-6500.

Pelekani, C., Snoeyink, V.L., 2000. Competitive adsorption between atrazine and methylene blue on activated carbon: the importance of pore size distribution. Carbon 38, 1423-1436.

Penners, N., Koopal, L., Lyklema, J., 1986. Interfacial electrochemistry of haematite (α-Fe_2O_3): homodisperse and heterodisperse sols. Colloids Surf. 21, 457-468.

Regazzoni, A.E., Blesa, M.A., Maroto, A.J., 1983. Interfacial properties of zirconium dioxide and magnetite in water. J. Colloid Interface Sci. 91, 560-570.

Ruiz-Reina, E., Gómez-Merino, A., Rubio-Hernández, F., García-Sánchez, P., 2003. Stern-layer parameters of alumina suspensions. J. Colloid Interface Sci. 268, 400-407.

Santos, G.M., Catellani, I.B., Santos, I.A., Guo, R., Bhalla, A.S., Padilha, J.E., Cótica, L.F., 2018. Microscopic description of the ferroism in lead-free $AlFeO_3$. Sci. Rep. 8, 1-8.

578 Satyanarayana, L., Reddy, K.M., Manorama, S.V., 2003. Nanosized spinel $NiFe_2O_4$: a novel material for the
579 detection of liquefied petroleum gas in air. Mater. Chem. Phys. 82, 21-26.
580 Seoane, B., Téllez, C., Coronas, J., Staudt, C., 2013. NH_2-MIL-53(Al) and NH_2-MIL-101(Al) in sulfur-containing
581 copolyimide mixed matrix membranes for gas separation. Sep. Purif. Technol. 111, 72-81.
582 Siddique, M.N., Ahmed, A., Tripathi, P., 2018. Electric transport and enhanced dielectric permittivity in pure and Al
583 doped NiO nanostructures. J. Alloys Compd. 735, 516-529.
584 Srivastava, M., Ojha, A.K., Chaubey, S., Materny, A., 2009. Synthesis and optical characterization of
585 nanocrystalline $NiFe_2O_4$ structures. J. Alloys Compd. 481, 515-519.
586 Swain, M., 2012. Chemicalize. org. ACS Publications.
587 Torad, N.L., Hu, M., Ishihara, S., Sukegawa, H., Belik, A.A., Imura, M., Ariga, K., Sakka, Y., Yamauchi, Y., 2014.
588 Direct synthesis of MOF‐derived nanoporous carbon with magnetic Co nanoparticles toward efficient
589 water treatment. Small 10, 2096-2107.
590 Vandevivere, P.C., Bianchi, R., Verstraete, W., 1998. Treatment and reuse of wastewater from the textile wet‐
591 processing industry: Review of emerging technologies. J. Chem. Technol. Biotechnol. 72, 289-302.
592 Wang, J., Wang, Y., Hu, H., Yang, Q., Cai, J., 2020. From metal-organic frameworks to porous carbon materials:
593 recent progress and prospects from energy and environmental perspectives. Nanoscale 12, 4238-4268.
594 Wang, L., Li, J., Wang, Y., Zhao, L., Jiang, Q., 2012. Adsorption capability for Congo red on nanocrystalline
595 MFe_2O_4 (M= Mn, Fe, Co, Ni) spinel ferrites. Chem. Eng. J. 181, 72-79.
596 Wang, Y., Zeng, L., Ren, X., Song, H., Wang, A., 2010. Removal of methyl violet from aqueous solutions using
597 poly (acrylic acid-co-acrylamide)/attapulgite composite. J. Environ. Sci. 22, 7-14.
598 Wu, Z., Zhong, H., Yuan, X., Wang, H., Wang, L., Chen, X., Zeng, G., Wu, Y., 2014. Adsorptive removal of
599 methylene blue by rhamnolipid-functionalized graphene oxide from wastewater. Water Res. 67, 330-344.
600 Xu, S., Lv, Y., Zeng, X., Cao, D., 2017. ZIF-derived nitrogen-doped porous carbons as highly efficient adsorbents
601 for removal of organic compounds from wastewater. Chem. Eng. J. 323, 502-511.
602 Xu, Y., Jin, J., Li, X., Song, C., Meng, H., Zhang, X., 2016. Adsorption behavior of methylene blue on
603 Fe_3O_4-embedded hybrid magnetic metal-organic framework. Desalination Water Treat. 57, 25216-25225.
604 Yagub, M.T., Sen, T.K., Afroze, S., Ang, H.M., 2014. Dye and its removal from aqueous solution by adsorption: a
605 review. Adv. Colloid Interface Sci. 209, 172-184.
606 Yang, S.J., Kim, T., Im, J.H., Kim, Y.S., Lee, K., Jung, H., Park, C.R., 2012. MOF-derived hierarchically porous
607 carbon with exceptional porosity and hydrogen storage capacity. Chem. Mater. 24, 464-470.
608 Yao, Y., Xu, F., Chen, M., Xu, Z., Zhu, Z., 2010. Adsorption behavior of methylene blue on carbon nanotubes.
609 Bioresour. Technol. 101, 3040-3046.
610 Yi, X., He, X., Yin, F., Yang, T., Chen, B., Li, G., 2020. NH_2-MIL-88B-Fe for electrocatalytic N_2 fixation to NH_3
611 with high Faradaic efficiency under ambient conditions in neutral electrolyte. J. Mater. Sci.
612 Yılmaz, E., Sert, E., Atalay, F.S., 2016. Synthesis, characterization of a metal organic framework: MIL-53 (Fe) and
613 adsorption mechanisms of methyl red onto MIL-53 (Fe). J. Taiwan Inst. Chem. Eng. 65, 323-330.
614 Yu, F., Bai, X., Liang, M., Ma, J., 2020. Recent progress on metal-organic framework-derived porous carbon and its
615 composite for pollutant adsorption from liquid phase. Chem. Eng. J., 126960.
616 Zhao, X., Liu, S., Tang, Z., Niu, H., Cai, Y., Meng, W., Wu, F., Giesy, J.P., 2015. Synthesis of magnetic
617 metal-organic framework (MOF) for efficient removal of organic dyes from water. Sci. Rep. 5, 11849.

Zhou, J., Ma, J., Sun, C., Xie, L., Zhao, Z., Tian, H., Wang, Y., Tao, J., Zhu, X., 2005. Low‐temperature synthesis of $NiFe_2O_4$ by a hydrothermal method. J. Am. Ceram. Soc. 88, 3535-3537.

Zhou, Y., Sun, L., Wang, H., Liang, W., Yang, J., Wang, L., Shuang, S., 2016. Investigation on the uptake and release ability of β-cyclodextrin functionalized Fe_3O_4 magnetic nanoparticles by methylene blue. Mater. Chem. Phys. 170, 83-89.

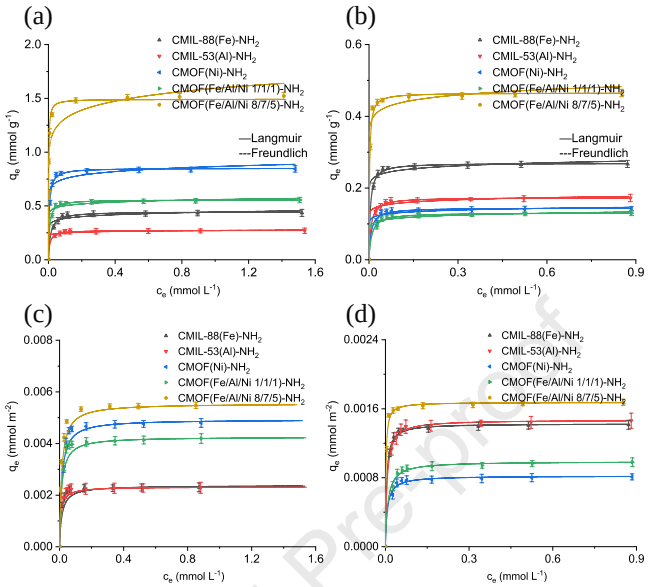

Figure 1. Adsorption isotherms of CMOFs-NH_2 normalized by the mass of adsorbents for (a) MB and (b) AR-73. The isotherms were fitted by Langmuir and Freundlich models. The adsorption isotherms were further normalized by the BET specific surface areas for (c) MB and (d) AR-73 to exclude the contribution of specific surface area to the adsorption capacities.

627

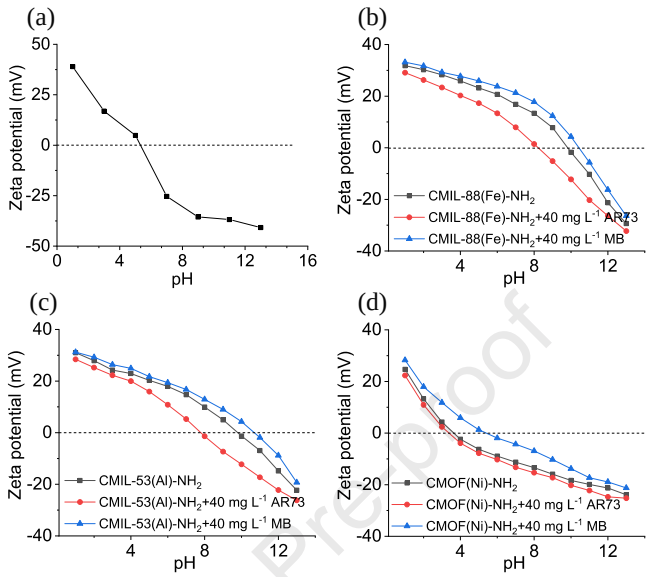

628 **Figure 2**. Zeta potential of (a) CMOF(Fe/Al/Ni 8/7/5)-NH_2, (b) CMIL-88(Fe)-NH_2, (c) CMIL-53(Al)-NH_2 and (d) CMOF(Ni)-NH_2

629 as a function of pH.

630

631 **Table 1.** Pseudo second-order kinetic parameters for adsorption of MB and AR-73 on CMOFs-NH_2 (C_0 = 40 mg L^{-1}, pH=7).

Kinetic parameters		CMIL-88(Fe)-NH_2	CMIL-53(Al)-NH_2	CMOF(Ni)-NH_2	CMOF(Fe/Al/Ni 1/1/1)-NH_2	CMOF(Fe/Al/Ni 8/7/5)-NH_2
MB adsorption	q_e (mmol g^{-1})	0.35	0.25	0.83	0.51	1.21
	v_0 (mmol g^{-1} h^{-1})	13.01	7.38	22.83	16.75	37.22
	R^2	0.993	0.974	0.980	0.991	0.993
AR-73 adsorption	q_e (mmol g^{-1})	0.26	0.16	0.13	0.11	0.45
	v_0 (mmol g^{-1} h^{-1})	8.02	5.08	4.46	2.95	13.96
	R^2	0.988	0.989	0.996	0.976	0.998

632

633

634 **Table 2.** Langmuir and Freundlich model parameters for adsorption of MB and AR-73 on CMOFs-NH_2 (pH=7).

Isotherm parameters		CMIL-88(Fe)-NH_2	CMIL-53(Al) -NH_2	CMOF (Ni)-NH_2	CMOF(Fe/Al/Ni 1/1/1)-NH_2	CMOF(Fe/Al/Ni 8/7/5)-NH_2
MB Langmuir constants	q_m (mmol g^{-1})	0.45	0.27	0.85	0.56	1.49
	b (L $mmol^{-1}$)	80.19	127.88	192.68	151.52	680.27
	R^2	0.991	0.998	0.997	0.996	0.994
MB Freundlich constants	K_f	0.44	0.27	0.87	0.56	1.59
	n^{-1}	15.94	26.87	16.56	21.30	11.84
	R^2	0.959	0.988	0.948	0.976	0.920
AR-73 Langmuir constants	q_m (mmol g^{-1})	0.27	0.17	0.14	0.13	0.47
	b (L $mmol^{-1}$)	234.19	161.81	147.28	115.07	531.91
	R^2	0.998	0.998	0.989	0.994	0.995
AR-73 Freundlich constants	K_f	0.28	0.18	0.15	0.13	0.49
	n^{-1}	21.71	19.15	19.63	15.61	21.23
	R^2	0.982	0.985	0.972	0.976	0.958

635

Declaration of interests

☒ The authors declare that they have no known competing financial interests or personal relationships that could have appeared to influence the work reported in this paper.

☐The authors declare the following financial interests/personal relationships which may be considered as potential competing interests: